Session II - 2.1

PROMINENCE DESTABILIZATION

CORONAL MASS EJECTIONS

3D RECONSTRUCTIONS

Nature of Prominences and their role in Space Weather
Proceedings IAU Symposium No. 300, 2013
B. Schmieder, J.-M. Malherbe & S. T. Wu, eds.

doi:10.1017/S1743921313010946

On the dynamics of eruptive prominences

Laura A. Balmaceda[1,6], Hebe Cremades[2], Guillermo Stenborg[3], Carlos Francile[4], Leonardo Di Lorenzo[5] and Fernando López[1]

[1]ICATE/CONICET-UNSJ,
CC 49, 5400 San Juan, Argentina
email: lbalmaceda@icate-conicet.gob.ar

[2]UTN - Facultad Regional Mendoza and CONICET, Mendoza, Argentina
[3]George Mason University, Fairfax, VA 22030, USA
[4]OAFA - Universidad Nacional de San Juan, San Juan, Argentina
[5]Universidad Nacional de San Luis, San Luis, Argentina
[6]Instituto Nacional de Pesquisas Espaciais, São José dos Campos, Brazil

Abstract. To contribute to the understanding of the physical mechanisms at work during the initial phase and early evolution of erupting prominences, we analyze combined observations from ground-based and space-borne instruments. We present two case studies, which occurred at two different phases of the solar cycle, namely on March 2, 2002 and on April 16, 2012. In particular, we show the results of a morphological and kinematical analysis and interpret them in terms of available theoretical models.

Keywords. Prominence dynamics, prominence eruption.

1. Introduction

Solar prominences have been studied for many decades using both ground-based and space-borne data. They usually show up in white-light coronagraph observations as a bright feature behind the leading edge (LE) of the associated CME, i.e., as the main part of the CME inner core (Webb & Hundhausen, 1987). They are also imaged onto the solar disk (as well as above the limb up to some fractions of a solar radii) at visible wavelengths in Hα, or in the extreme ultraviolet range as in HeII or highly-ionized Fe lines. Combined observations from such instruments provide a great opportunity to get insight on their early development. During the SOHO/LASCO (Brueckner *et al.*, 1995) era, it was well established that CMEs and filament/prominence eruptions are strongly related (Srivastava *et al.*, 1999, Gopalswamy *et al.*, 2003; Jing *et al.*, 2004, and references therein).

Prominences are believed to be related to the formation of a magnetic flux rope, which eventually erupts to form the CME (Low, 2001). Thus, the study of their kinematic profile during their onset and early rise in the low corona at high cadences provides crucial information on the forces/physical mechanisms that trigger/drive the eruption.

On a theoretical aspect, many models have been developed to describe the CME initiation. In particular, Chen (1989) and Chen (1996) considered a line-tied current-carrying loop, e.g., a flux rope, holding a prominence at its bottom, and derived the total force exerted on its apex. Given that a prominence is generally stable for weeks before erupting, they proposed that a flux rope can be accelerated and erupt when new poloidal flux is injected into the system. An instability, named *torus instability* from laboratory plasma experiments (Kliem & Török, 2006), would take place in the flux rope due to the "toroidal force" and eventually act as the trigger mechanism for the eruption.

In this work, we use data from two ground-based solar instruments in combination with satellite images of two particular events, which we further contrast with the theoretical model developed by Chen (1996) to shed light into the dynamics of prominence eruptions during their early stages.

2. The observations

The two ground-based instruments are operating in San Juan, Argentina (31.8 S, 69.3 W, at 2400 m of altitude) since 1999. The observing time window runs between roughly 12 UT and 20 UT. MICA (Mirror Coronagraph for Argentina, Stenborg *et al.* 1999) is an internally-occulted mirror coronagraph with a plate scale of 3.6"/pixel. Two auxiliary devices allow the constant monitoring of the atmospheric conditions and hence its automatic operation. It images the solar corona at a nominal cadence of $\sim$ 1 min between 1.05 and 2.0 $R_\odot$ in the Fe XIV line (at 530.3 nm, hereafter green line) and in the continuum emission (at 526.0 nm) using interference filters that have a full width at half maximum (FWHM) passband of 0.13 and 1.1 nm, respectively. On the other hand, HASTA† (H-alpha Solar Telescope for Argentina, Bagalá *et al.* 1999) is a full-disk imager, with a plate scale of $\sim$2"/pixel operating in two cadence modes: 90 seconds in patrol mode and 3 seconds in high speed mode. It images the solar disk in the Hα emission line at 656.27 nm with a filter of 0.03 nm (FWHM).

Unfortunately, the detection of faint dynamic events in MICA observations is not a straightforward task due to the highly varying atmospheric conditions at the observing site. Therefore, in order to help reveal the events of interest we first process the images with a customized version of the wavelet-based technique developed by Stenborg & Cobelli (2003) to clean the images and thus increase the relative intensity contrast of the coronal features in the images (the detailed description of the devised technique will appear elsewhere).

2.1. *Event A: March 2, 2002*

On March 2, 2002, the onset phase of an erupting prominence was identified in both HASTA Hα and MICA green-line images. The prominence initial height (Z_{p_0}) in HASTA observations, as measured from the disk center at 14:24 UT, was 1.05 $R_\odot$, the separation between the footpoints being $\sim$0.3 $R_\odot$. These measurements were confirmed with observations from the Extreme Ultraviolet Imaging Telescope (EIT, Delaboudinière *et al.*, 1995) onboard SOHO. The prominence was a long-lived one, which had been observed in HASTA images since some weeks prior to the eruption. The eruption gave rise to a well structured three-part CME observed later in the LASCO-C2 and -C3 coronagraphs (Bruecker *et al.*, 1995) as seen in the composite of MICA and LASCO-C2 images (Fig. 1, left panel). From MICA images we could determine the main acceleration phase of the prominence eruption. The prominence shows a gradual increase during its early phase (open circles in Fig. 2, top left panel). At distances beyond $\sim$3.5 $R_\odot$, the height–time profile is approximately linear with a constant velocity of $\sim$1000 km s^{-1}.

2.2. *Event B: April 16, 2012*

At the time of the event, the coronagraph's observing mode was set to take images only in the green-line continuum, allowing for a cadence of 40 seconds. An erupting prominence was first observed above the eastern limb at $\sim$17:30 UT. We identified this eruption as the initial phase of a CME observed later in LASCO-C2 and C3 data (see in Fig.1, central

† http://www.oafa.fcefn.unsj-cuim.edu.ar/Hasta/

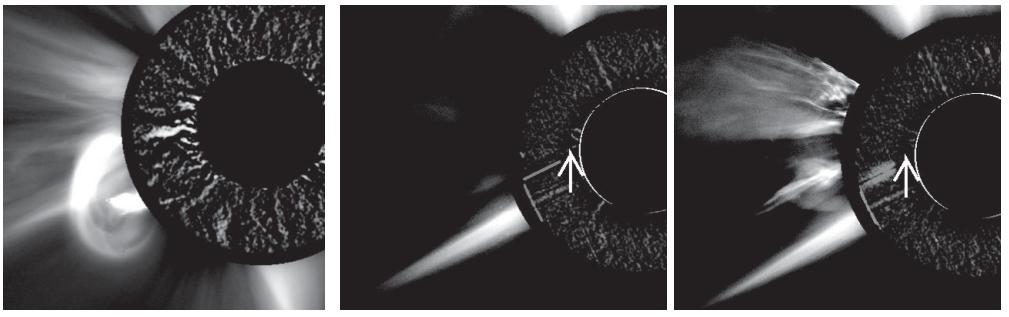

Figure 1. Composite of quasi-simultaneous MICA and LASCO-C2 images. *Left:* Event A, at ∼15:30 UT. *Center:* Event B, early development of the prominence eruption (∼17:36 UT). *Right:* Event B at ∼18:24 UT. The arrows pinpoint the prominence legs.

and right panels the composite of MICA and LASCO-C2 FOVs). The eruption develops gradually in the lower corona. A large amount of the prominence material is observed to drain back to the Sun in HASTA images. At higher distances from the Sun, the CME LE moves at ∼1000 km s^{-1}, with an acceleration of −30 m s^{-2} (as determined from the corresponding height–time plot for heights $> 2R_\odot$, at ∼71° position angle. See Fig. 2, bottom left panel, where the LASCO measurements are indicated by crosses).

3. Comparison with a theoretical model

In the integrated MHD approach developed by Chen (1996), the modeled flux rope is described by a non-axisymmetric geometry, with an average major radius of curvature during expansion R, stationary footpoints with separation S_f, and a non-uniform minor radius a. The initial structure is assumed to be in equilibrium. The conditions for the ambient coronal field are specified by an independent model. The eruption is triggered by the injection of poloidal magnetic flux whose profile is imposed (a generic pulse whose variation is described by Eq. 9 in Chen & Kunkel, 2010). The flux rope is driven mainly by the Lorentz force arising from the toroidal currents and is assumed to remain connected to the solar surface. The model solves two coupled differential equations (Eq. 2 and 9 in Chen, 1996) that describe the forces acting on the major and minor radii and are evaluated in the apex of the structure. These are: Lorentz force arising from the poloidal component of the magnetic field and the downward tension due to the toroidal component, the gravitational force, the drag force, and the pressure gradient.

The geometric characteristics of the initial flux rope, as well as the initial mass derived from observational data are used to constrain the model following the methodology described in Chen *et al.* (2006). The height of the CME LE is given by $Z_{LE} = Z + 2a_a$, while the prominence height can be obtained from: $Z_p = Z - a$ and the prominence footpoint separation is related to the flux rope footpoint separation by $S_p = S_f - 2a_f$. Here, Z denotes the height of the apex and the subindices f and a indicate the flux rope and apex parameters.

From solar images we determine the observed quantities: S_p and Z_p. We estimate the CME mass using LASCO data and following the Vourlidas *et al.* (2010) technique. We deduce Z_0=1.6×10^5 km, S_0=1.2×10^5 km and M_0= 10^{16} g for Event A, and Z_0=8×10^4 km, S_0=1×10^4 km, M_0= 10^{15} g for Event B. We consider a maximum flux injection rate of $d\phi/dt_{max}$=10^{19} Mx s^{-1} in both cases. In order to find the time constants that define the flux injection profile (set as free parameters in the model), the genetic algorithm PIKAIA

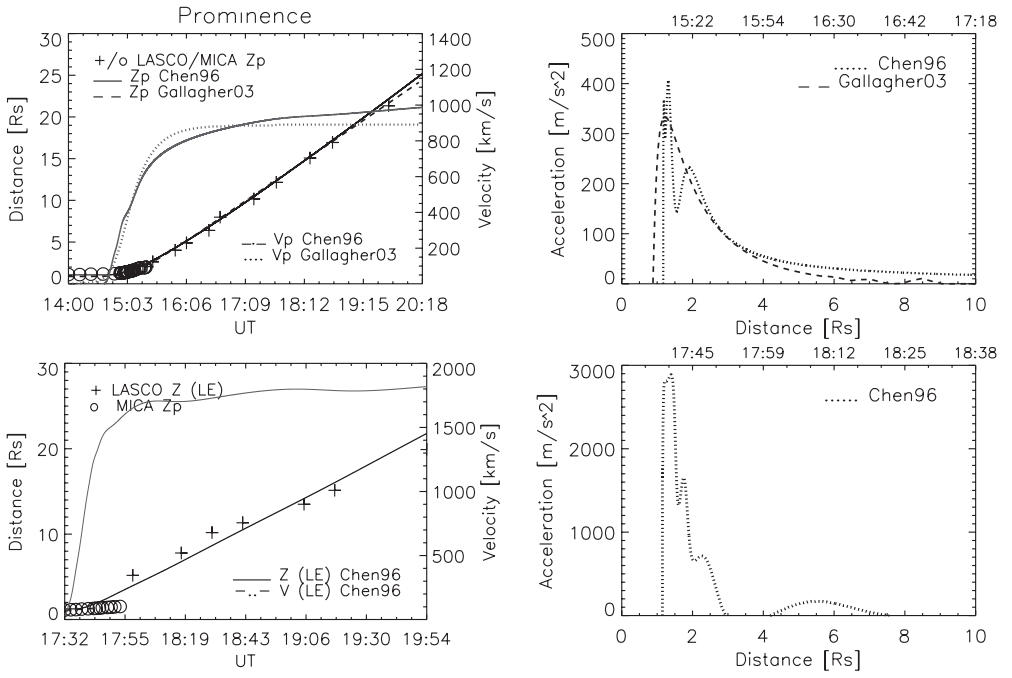

Figure 2. Height-time plot for the prominence and for the CME leading edge: Event A (top left), Event B (bottom left). The solid curves correspond to the fitting of the observations by the given models. Right panels: Acceleration profile derived from the models for Event A (top) and Event B (bottom).

by Charbonneau (1995) is used. The model is set to fit the observations up to ∼20 $R_\odot$ by minimizing a χ^2-function.

The comparison between the observed heights and the results of the model is shown in Fig.2 (left panels) for both events. For Event A (top panel), the model is evaluated by comparing the measured prominence heights through MICA and LASCO FOVs. The results of the model describe fairly well the observations (solid line). The velocity exhibits a rapid increase at heights < 2 $R_\odot$ (dash-dotted line). This is also in good agreement with the velocity profile obtained assuming the hypothesis of a exponential varying acceleration suggested by Gallagher *et al.* (2003) (dashed line for the H-T and dotted line for the velocity-time curve in Fig. 2 top left panel). The acceleration reaches a maximum of ∼300–400 m s^{-2} when the prominence top is at ∼1.5 $R_\odot$ (∼15:05 UT, Fig. 2 top right panel). For Event B (Fig. 2, bottom panel) the prominence front is only well detected in MICA FOV (open circles). It is seen to expand gradually and erupt after reaching ∼1.7 $R_\odot$. Its top is not clearly discernible in LASCO-C2 FOV. The model is then evaluated by comparing only the CME LE in LASCO FOV (crosses). MICA observations are used only to constraint the initial morphological parameters of the flux rope. The modeled acceleration profile shows a main acceleration phase also at low heights with a peak at ~ 1.7 $R_\odot$ and a residual acceleration phase at distances beyond 4 $R_\odot$ (bottom right panel). These results, however, should be further contrasted using complementary data from current missions. A complete analysis of these events will be published in an upcoming paper.

4. Concluding remarks

In this work, we have studied the evolution of two erupting prominences associated to CMEs using combined data from ground and space. We have also compared these observations with the model by Chen (1996) of the eruption of a flux rope and found good agreement.

Despite the limitations imposed by the observing time window and weather conditions, the ground-based data used in this work proved to be a suitable complement to existent space-based EUV and white-light coronagraph data, in particular to SOHO/EIT observations (the EIT FOV was limited to 1.4 $R_\odot$ with a nominal temporal cadence of only 12 min), and to LASCO observations before the advent of STEREO (Kaiser *et al.*, 2008) and SDO (Pesnell *et al.*, 2012) missions (the extended field of view of the MICA coronagraph fills the gap between the outer edge of AIA FOV and the inner edge of LASCO-C2). We plan to perform a morphological and kinematical analysis of a selection of events that occurred at different phases of solar cycle 23, and check the results against theoretical models, to shed light on the dynamics of eruptive phenomena, in particular during their early stages.

Acknowledgements

L.B. and H.C. are members of the Carrera del Investigador Científico of CONICET. L.B. thanks the organizers and the IAU for the financial support to attend the Symposium.

References

Bagalá, L. G., Bauer, O. H., Fernández Borda, R., *et al. Magnetic Fields and Solar Processes*, 1999, ESA Special Publication, 448, 469
Brueckner, G. E., Howard, R. A., Koomen, M. J., *et al.* 1995, *Sol. Phys.* 162, 357–402
Charbonneau, P. 1995, *ApJS*, 101, 309
Chen, J. 1989, *ApJ* 338, 453–470
Chen, J. 1996, *JGR*, 101, 27499–27520
Chen, J., Marqué, C., Vourlidas, A., Krall, J., & Schuck, P. W. 2006, *ApJ*, 649, 452–463
Chen, J. & Kunkel, V. 2010, *ApJ*, 717, 1105–1122
Delaboudinière, J.-P., Artzner, G. E., Brunaud, J., *et al.* 1995, *Sol. Phys.* 162, 291–312
Gallagher, P. T., Lawrence, G. R., & Dennis, B. R. 2003, *ApJL*, 588, L53–L56
Gopalswamy, N., Shimojo, M., Lu, W., *et al.* 2003, *ApJ*, 586, 562–578
Jing, J., Yurchyshyn, V. B., Yang, G., Xu, Y., & Wang, H. 2004, *ApJ*, 614, 1054–1062
Kaiser, M. L., Kucera, T. A., Davila, J. M., *et al.* 2008, *Sp. Sci. Rev.*, 136, 5–16
Kliem, B. & Török, T. 2006, *Phys. Rev. Let.*, 96, 25, 255002
Low, B. C. 2001, *JGR*, 106, 25141–25164
Pesnell, W. D., Thompson, B. J., & Chamberlin, P. C. 2012, *Sol. Phys.*, 275, 3–15
Srivastava, N., Schwenn, R. & Stenborg, G. 1999, 8th SOHO Workshop: Plasma Dynamics and Diagnostics in the Solar Transition Region and Corona, ESA Special Publication, 446, 621
Stenborg, G., Schwenn, R., Srivastava, N., *et al.* 1999, *Sp. Sci. Rev.*, 87, 307–310
Stenborg, G. & Cobelli, P. J. 2003, *Astron. Astroph.*, 398, 1185–1193
Vourlidas, A., Howard, R. A., Esfandiari, E., *et al.* 2010, *ApJ*, 722, 1522–1538
Webb, D. F. & Hundhausen, A. J. 1987, *Sol. Phys.*, 108, 383–401